Analytica Chimica Acta 1175 (2021) 338749

Contents lists available at ScienceDirect

Analytica Chimica Acta

journal homepage: www.elsevier.com/locate/aca

Polymer-dispersed reduced graphene oxide nanosheets and Prussian blue modified biosensor for amperometric detection of sarcosine

Thenmozhi Rajarathinam [a, 1], Minho Kwon [b, 1], Dinakaran Thirumalai [a, **], Seonghye Kim [c], Seulah Lee [d], Jang-Hee Yoon [e], Hyun-jong Paik [b], Suhkmann Kim [c], Jaewon Lee [d], Hong Koo Ha [f, ***], Seung-Cheol Chang [a, *]

[a] Department of Cogno-Mechatronics Engineering, College of Nanoscience and Nanotechnology, Pusan National University, Busan, 46241, Republic of Korea
[b] Department of Polymer Science and Engineering, Pusan National University, Busan, 46241, Republic of Korea
[c] Department of Chemistry, Pusan National University, Busan, 46241, Republic of Korea
[d] College of Pharmacy, Pusan National University, Busan, 46241, Republic of Korea
[e] Busan Center, Korea Basic Science Institute, Busan, 46241, Republic of Korea
[f] Department of Urology and Biomedical Research Institute, Pusan National University Hospital, Pusan National University, Busan, 49241, Republic of Korea

HIGHLIGHTS

- A new polymer dispersant synthesized to disperse reduced graphene oxide (P-rGO).
- P-rGO and Prussian blue utilized for amperometric sarcosine biosensor.
- SOxENs prepared using P-rGO and sarcosine oxidase (SOx).
- High selectivity against major interferents in human urine.
- The designed biosensor is more suitable for non-invasive prostate cancer diagnosis.

GRAPHICAL ABSTRACT

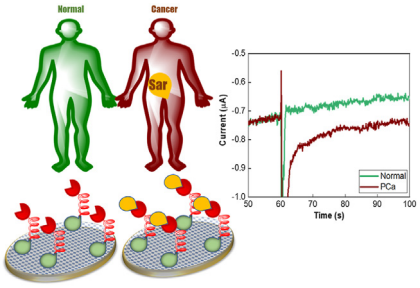

ARTICLE INFO

Article history:
Received 4 May 2021
Received in revised form
2 June 2021
Accepted 8 June 2021
Available online 9 June 2021

Keywords:
Amperometric biosensor
Prostate cancer biomarker
Polymer dispersed rGO
Prussian blue
Sarcosine

ABSTRACT

A new disposable amperometric biosensor for sarcosine (Sar, a biomarker for prostate cancer) was designed based on screen-printed carbon electrodes, Prussian blue, polymer dispersed reduced graphene oxide (P-rGO) nanosheets, and sarcosine oxidase (SOx). Poly(sodium 4-styrenesulfonate-*r*-LAHEMA) denoted as PSSL was newly synthesized as dispersant for rGO. The P-rGO was utilized for SOx immobilization, the sulfonate and disulfide functionalities in PSSL enable physical adsorption of SOx and its bioactivity and stability properties were improved. The biosensor was optimized by various enzyme concentration, applied potential, and operating pH. Under the optimized conditions, the biosensor exhibited maximum current responses within 5 s at an applied potential of −0.1 V *vs.* integrated Ag/AgCl reference electrode. The biosensor had a dynamic linear range of 10–400 μM, with a sensitivity of 9.04 μA mM^{-1} cm^{-2} and a low detection limit of 0.66 μM (S/N = 3). Additionally, the biosensor possesses strong anti-interference capability, high reproducibility, and storage stability over 3 weeks. Furthermore, its clinical applicability was tested in urine samples from both prostate cancer patients and healthy

* Corresponding author.
** Corresponding author.
*** Corresponding author.
E-mail addresses: dinakaran@pusan.ac.kr (D. Thirumalai), hongkooha@pusan.ac.kr (H.K. Ha), s.c.chang@pusan.ac.kr (S.-C. Chang).
[1] These authors contributed equally to this work.

https://doi.org/10.1016/j.aca.2021.338749

control, and the analytical recoveries were satisfactory. Therefore, this biosensor has significant potential in the rapid and non-invasive point-of-care testing for prostate cancer diagnosis.

1. Introduction

[2]Prostate cancer (PCa) is a malignancy that is usually asymptomatic at the initial stage but is associated with high mortality rates in the advanced stages. Therefore, its early detection is essential for improving the survival rates. Over the last two decades, prostate-specific antigen has been validated as a protein biomarker for PCa [1]. Prostate cancer specific biomarker is essential to identify the PCa and to reduce complications from prostatic biopsy because prostate-specific antigen can be elevated in patients with non-cancerous lesion including prostatitis or benign prostatic hyperplasia. A study of urine metabolites in patients has contributed to the discovery of a range of metabolites that are elevated in PCa, including sarcosine (Sar) [2]. Depending on the aggressiveness of the PCa, Sar concentration in the urine samples could exceed several micromoles [3].

Analytical methods reported for Sar detection include colorimetry, spectrometry, and liquid chromatography-mass spectrometry. However, these methods have drawbacks such as requirement of costly instruments and/or skilled operator, complex sample pretreatment steps, low sensitivity, and susceptibility to interferences [4]. Since electrochemical biosensors are free from these drawbacks, they are promising for rapid, simple, and accurate Sar determination in early and non-invasive diagnosis of PCa. Enzyme-based biosensors are preferable for the selective detection of target analytes. Sarcosine oxidase (SOx) is employed as a biocatalyst in enzyme-based amperometric biosensors. For instance, the SOx was utilized as one of the enzymes along with creatine amidinohydrolase to construct creatine biosensor [5]. The SOx enzyme alone could be used to fabricate the Sar biosensor [6]. The SOx (Eq. (1)) convert Sar to glycine, formaldehyde, and hydrogen peroxide (H_2O_2).

$$Sar + O_2 + H_2O \xrightarrow{SOx} Glycine + Formaldehyde + H_2O_2 \quad (1)$$

$$H_2O_2 \rightarrow O_2 + 2H^+ + 2e^- \quad (2)$$

Quantification of H_2O_2 produced in Eq. (1) provides an indirect measure of Sar concentration in serum or urine samples. Other researchers have mainly focused on H_2O_2 oxidation (Eq. (2)), approximately at +0.6 V. Here, to exclude electrochemically active interferents, we assessed the reduction of H_2O_2 in the negative region with only a low applied potential instead. Another problem is that the immobilization of SOx alone prompts its easy denaturation, resulting in decreased catalytic activity and stability of the enzyme. In this context, nanomaterials may improve the catalytic properties and stability of SOx [7,8]. For instance, SOx immobilized on zeolitic imidazolate framework-8 and polyvinyl alcohol-silica-AuNP films demonstrated improved catalytic properties and retained the bioactivity of SOx [9,10]. Briefly, improvement in the detection of Sar at lower concentrations and the sensitivity at a low applied potential is essential.

When modified onto the working electrode, Prussian blue (PB, a mixed-valence iron compound) promotes high catalytic activity and selectivity for H_2O_2 reduction compared with platinum modifications [11]. The sensitivity, selectivity, and stability properties of PB favor easy H_2O_2 reduction at very low applied potentials. However, the possibility of applying a low potential in H_2O_2 reduction has been rarely investigated [12].

Graphene-based architectures with two-dimensional networks possess unique properties that are useful in biosensors, such as high catalytic efficiency, ease of functionalization, and the ability to accommodate guest molecules [13]. Reduced graphene oxide (rGO) has better metallic properties than GO due to the sp^2 conjugations, and it offers several advantages as an ideal support material for enzymatic biosensors [14]. Nevertheless, its application is limited by the easy aggregation in aqueous solvents due to van der Waals interactions within the rGO sheets. To overcome these problems, rGO could be dispersed by physical methods, covalent methods, and non-covalent methods. The covalent method alters the sp^2 structure in rGO lattices, which, however, leads to defects and loss of electronic properties. On the other hand, noncovalent methods retain the structure and electronic properties of rGO and are more efficient than other methods [15]. Therefore, the noncovalent methods for rGO dispersion could lead to good dispersibility, binding capacity, and biosensing properties.

Many polymers have been used as non-covalent dispersants for rGO, such as poly(sodium 4-styrenesulfonate) (PSS) [16], sulfonated polyaniline [17], polyimide [18], amine-terminated polystyrene [19], tri-block copolymers [20], and pyrene-terminated polymers [21]. PSS co-polymers possess amphiphilic functionalities that readily interact with both the hydrophobic rGO sheets and the hydrophilic solvent molecules [22]. Moreover, no additional reagents or cross-linking agents are required. Many previous studies have utilized Nafion, a perfluorinated sulfonate ionomer, as an anti-interfering film on biosensors [23]. The electronegative sulfonate groups in the PSS co-polymers are similar to the sulfonate groups in Nafion and could presumably exclude interfering signals. These appealing properties of PSS based co-polymers with the rGO platform might mitigate the conductivity loss and open new avenues for the design of biosensors.

Herein, we describe a simple method to fabricate an amperometric Sar biosensor employing screen-printed carbon electrodes (SPCEs). A schematic illustration of the proposed Sar biosensor is shown in Scheme 1. The SPCEs were modified with PB (PB/SPCEs). rGO dispersed with a newly synthesized polymer dispersant, poly(sodium 4-styrenesulfonate-r-LAHEMA), PSSL was denoted as P-rGO. The P-rGO was pre-incubated with SOx for 10 min to favor physical interactions between the SOx and P-rGO. The mixture of P-rGO and SOx enzyme (SOx enzyme nanosheets, SOxENs) was then drop-casted onto the PB/SPCEs and termed SOxENs/PB/SPCE. P-rGO provides a large surface area and a biocompatible frame for

[2] Abbreviations: azobisisobutyronitrile (AIBN), sodium 4-styrenesulfonate (SS), poly(sodium 4-styrenesulfonate) (PSS), lipoic acid (LA), 2-hydroxyethyl methacrylate (HEMA), graphene oxide (GO), reduced graphene oxide (rGO), Poly(sodium 4-styrenesulfonate-*r*-LAHEMA) dispersed reduced graphene oxide (P-rGO), dichloromethane (DCM), N,N-dicyclohexylcarbodiimide (DCC), dimethyl sulfoxide (DMSO), 4-dimethylaminopyridine (DMAP), screen-printed carbon electrode (SPCE), sarcosine (Sar), sarcosine oxidase (SOx), Prussian blue (PB), prostate cancer (PCa), phosphate-buffered solution (PBS), field-emission scanning electron microscope (FE-SEM), energy-dispersive X-ray spectroscopy (EDS), transmission electron microscopy (TEM), X-ray photoelectron spectroscopy (XPS), cyclic voltammetry (CV), electrochemically active surface area (ECSA), chronoamperometry (CA), electrochemical impedance spectroscopy (EIS), limit of detection (LOD).

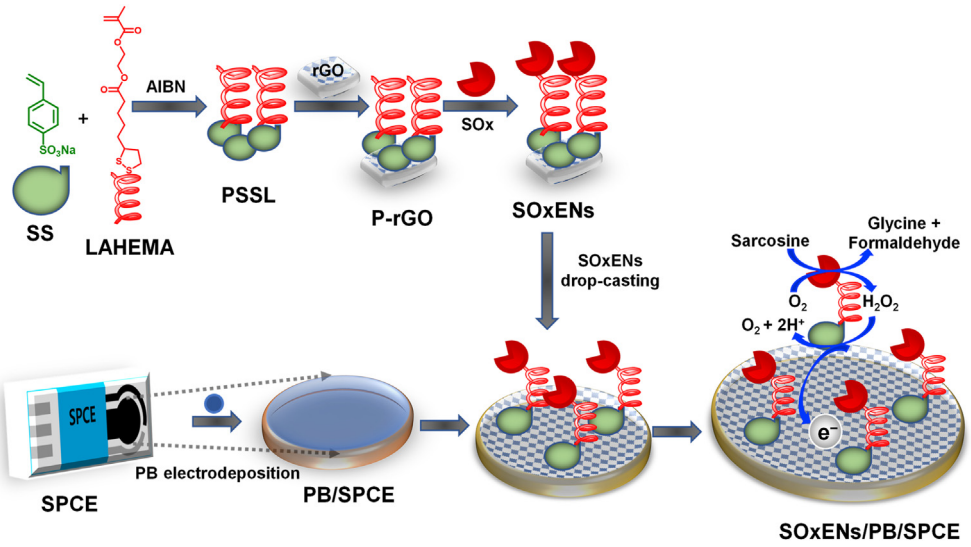

Scheme 1. Schematic illustration of proposed Sar biosensor.

trapping large amounts of SOx. The combined properties of PB and P-rGO with SOx biocatalyst improved the performance of the amperometric Sar biosensor compared to other biosensors reported in the literature.

2. Experimental

2.1. Reagents and chemicals

The following reagents and chemicals were purchased from Sigma-Aldrich (USA): sarcosine oxidase (SOx, EC 1.5.3.1) from *Bacillus* species, sarcosine (Sar), potassium ferricyanide ($K_3[Fe(CN)_6]$), 2-hydroxyethyl methacrylate (HEMA), 4-dimethylaminopyridine (DMAP), lipoic acid (LA), dichloromethane (DCM), N,N-dicyclohexylcarbodiimide (DCC), magnesium sulfate ($MgSO_4$), azobisisobutyronitrile (AIBN), iron (III) chloride ($FeCl_3$), sodium 4-styrenesulfonate (SS), sodium phosphate monobasic (NaH_2PO_4), dimethyl sulfoxide (DMSO), hydrazine monohydrate, sodium phosphate dibasic (Na_2HPO_4), and potassium chloride (KCl). Graphene oxide (GO) was supplied by Nanosolution (South Korea). Phosphate-buffer solution (PBS, 50 mM) with varied pH was made by combining NaH_2PO_4 with Na_2HPO_4 and KCl (100 mM) to increase the ionic strength of the working buffer. All other reagents used were of analytical grade and utilized as received without any further purification steps. All the solutions were made using three times distilled water (18 MΩ) purified from a Milli-Q water purifying system.

2.2. Fabrication of sarcosine biosensors

2.2.1. PB electrodeposition

Screen-printed carbon electrodes (SPCEs, 4 mm diameter; model C11L) were procured from Metrohm DropSens (Oviedo, Spain). The SPCEs were cleaned in 100 mM PBS (pH 7.0) and then underwent 40 cycles from −0.6 to +1.6 V at 100 mV s^{-1} to increase the surface functionalities. After surface cleaning, PB electrodeposition was carried out at a potential of +0.4 V for 60 s in 5 mM $FeCl_3$ & $K_3[Fe(CN)_6]$, and the electrolytes of 100 mM HCl and 100 mM KCl. For even and stable film growth, the deposited PB films were activated in the HCl and KCl electrolyte solution, cycling the applied potential from −0.05 to 0.35 V at a scan rate of 50 mV s^{-1} [12]. The resulting biosensor was named PB/SPCE.

2.2.2. Synthesis of P-rGO

Synthesis of LAHEMA: HEMA (5.82 mmol), DMAP (0.969 mmol), and LA (4.85 mmol) were injected to a 100 mL round-bottom flask, dissolved in DCM (15.0 mL) with N_2 gas purge, and kept at 0 °C. A DCC solution (5.82 mmol) in DCM (85.0 mL) was slowly injected dropwise, followed by stirring at 25 °C for 24 h. The final precipitate was collected using a nylon filter. The samples were washed with deionized water, dried with $MgSO_4$, and vacuum-evaporated to remove organic contaminants. Finally, the LAHEMA product was obtained.

Synthesis of PSSL: AIBN (0.0425 mmol) was injected into a 100 mL round-bottom flask, which was subsequently backfilled with N_2 gas using a vacuum pump. SS (7.64 mmol), LAHEMA (0.850 mmol), and DMSO (15.0 mL) were injected into the flask and stirred at 90 °C for about 3 h. After the polymerization reaction, the solution was precipitated with acetone. The mixture was then centrifuged and dried at 25 °C under vacuum overnight to obtain poly(SS-*r*-LAHEMA) named as PSSL.

In a 500 mL round-bottom flask, GO (40.0 mg) was dispersed in deionized water (400 mL) with mild shaking, and then PSSL (400 mg) was added. Hydrazine monohydrate (4.00 mL) was slowly injected into the reaction mixture. The resultant mixture was sonicated using a bath-type sonicator (400 W) for 30 min and then stirred at 70 °C oil bath for 6 h. The solution was sonicated for 30 min and the obtained product was centrifuged at 33,800×*g* for 30 min to remove the free polymers, and the pellet was collected.

2.2.3. Preparation of SOxENs

Approximately 3 μL of P-rGO (0.2 mg/mL) was pre-incubated with an equal volume of SOx (0.4 mg/mL) for 10 min to prepare the SOxENs. Then, approximately 6 μL of the prepared SOxENs was drop-cast over the PB/SPCEs surface. The large surface area of P-rGO favors SOx loading by physical adsorption or entrapment, resulting in the formation of SOxEN. The electrode was dried at 4 °C overnight and labelled SOxENs/PB/SPCEs.

2.3. Instrument and measurements

Surface analysis of the electrodes was performed using field-emission scanning electron microscopy (FE-SEM, Zeiss SUPRA 25) with energy-dispersive X-ray spectroscopy (EDS). Transmission electron microscopy (TEM) images were acquired using a HITACHI

H-7600 TEM instrument. X-ray photoelectron spectroscopy (XPS) analysis was performed using a K-Alpha X-ray photoelectron spectrometer system (Thermo Scientific, Waltham, MA, USA). Cyclic voltammetry (CV) and electrochemical impedance spectroscopy (EIS) measurements were taken using a potentiostat (CH Instruments, USA, model 604E). Chronoamperometry (CA) measurements were carried out using an electrochemical apparatus (Compactstat, Ivium Technologies B.V., Eindhoven, The Netherlands).

A disposable 2-mL electrochemical cell was set up to take the CV measurements. The biosensor was initially placed in a 2 mL of 100 mM KCl containing 5 mM $K_3[Fe(CN)_6]$ with potential sweeps from −0.2 to +0.6 V at different scan rates. The EIS analysis was studied in the same solution in the frequency range (100 kHz−0.1 Hz) at the formal potential of $K_3[Fe(CN)_6]$, which is AC potential amplitude (5 mV) on a DC potential (250 mV). For CA, the biosensor was connected via a potentiostat, approximately 60 μL of PBS was kept onto the electrode surface and polarized at −0.10 V. Following the achievement of a stable baseline response, 20 μL of Sar solution was introduced, and the current responses were measured across time. To obtain the calibration curves, the measurements were taken multiple times with various concentrations of Sar.

2.4. Preparation of real urine samples

The clinical applicability of the proposed biosensor was evaluated by a standard addition method using human urine samples. The normal and PCa urine samples were prepared at various dilutions (with distilled water) and investigated. The diluted urine samples with negligible interferences were chosen to minimize the matrix effects. The urine samples (4 × 100 μL) spiked by the addition of 100 μL of known concentrations of Sar (0.0, 10, 25, and 50 μM), was prepared and CA measurements were carried out. The dilution factors of the spiked urine were 15. The cumulative Sar concentrations found in spiked urine were calculated in the same way that the linear calibration plots were calculated. This study was reviewed carefully and approved by the Pusan National University Hospital (PNUH IRB No.1802-004-063), and all the experiments were carried out following the approved guidelines. Each patient signed an informed consent form.

For comparison with the biosensor results, Sar concentrations in normal and PCa urine samples were estimated using a standard sarcosine assay kit (cat. ab65338; Abcam) as per the manufacturer's protocol.

3. Results and discussion

3.1. Physicochemical characterizations

The electrodes were characterized by FE-SEM with EDX microanalysis and TEM to assess the morphological changes after each modification and are given in Fig. 1. The PB-modified SPCE had a slightly smoother surface with uniformly distributed PB nanospheres/cluster-like structures than the bare SPCE, which had a rugged surface and a non-smooth morphology (Fig. 1a and b). The P-rGO/SPCEs had evenly distributed rGO sheets with a two-dimensional layered morphology without any aggregated structures (Fig. 1c). Both PB nanospheres and rGO sheet-like structures were observed on the P-rGO/PB/SPCE (Fig. 1d). After SOxENs immobilization, the surface became relatively smoother with small globular structures, as shown in Fig. 1e. The ratios of major elements were analyzed using EDS and elemental mapping. SOxENs/PB/SPCE shows characteristic carbon (C) and oxygen (O) peaks due to the SPCE and iron (Fe) and nitrogen (N) components, confirming PB electrodeposition; and the additional sulfur (S) peak is presumably due to disulfide and sulfonate groups in PSSL. (Figs. S1a and b). In TEM observation, rGO dispersed without PSSL demonstrates multi-stacked nanosheets (Fig. S2a). In contrast, the sample dispersed with PSSL shows even distribution of thin rGO films without aggregates, indicating stable dispersion properties of PSSL (Fig. S2b). The inset photographs show more aggregated rGO structures (Fig. S2a inset) and homogeneously dispersed rGO (Fig. S2b inset). Additionally, the hydrophilic PSSL serves as a frame which interacts with the hydrophobic rGO nanosheets through π-π stacking. The hydrophilicity of the PSSL is attributed to the sulfonate functionalities [24], which result in stable dispersions after more than six months without any precipitation.

XPS measurements were used to confirm the electronic states and surface chemical composition of the variously modified electrodes in a detailed manner. The survey spectrum (Fig. 2) of bare SPCE displays only C and O peaks, while that of PB/SPCE features additional Fe2p and N1s peaks. P-rGO/SPCE also demonstrates characteristic C and O peaks with an additional S2p peak, which is ascribed to the disulfide groups in the PSSL. P-rGO/PB/SPCE shows peaks similar to those of PB/SPCE and P-rGO/SPCE. Interestingly, the C/O ratios of P-rGO/PB/SPCE and SOxENs/PB/SPCE were calculated to be 7:1 and 5:1, respectively. The decreased C/O ratio in the latter illustrates that significant deoxygenation occurred by Fe^{2+} reduction, resulting in abundant oxygen functional groups on the rGO planes that also serve as attachment sites for SOx. The atomic percentages of Fe in PB/SPCE, P-rGO/PB/SPCE, and SOxENs/PB/SPCE were 15.5%, 6.8%, and 2.8%; and those of N were 25.6%, 18.1%, and 18.3%, respectively. The Fe and N constituents confirmed the existence of PB. The atomic percentages of S in P-rGO/SPCE, P-rGO/PB/SPCE, and SOxENs/PB/SPCE were 0.3%, 0.4%, and 0.6%, respectively, owing to the sulfonate and disulfide functionalities in the PSSL.

The high-resolution C1s & O1s spectra of all modified electrodes are shown in Fig. S3. The deconvoluted C1s region (Fig. S3a) of bare SPCE features two peaks at 284.6 (C═C in sp^2 hybridization) and 285.7 eV (C−O/C−OH groups). PB/SPCE reveals similar peaks to bare SPCE, but with an additional peak at 293.6 eV ascribed to π−π* satellite bonds. P-rGO/SPCE and P-rGO/PB/SPCE display same peaks as bare SPCE, plus another one at 286.0 eV (C−O−C epoxy group of rGO). SOxENs/PB/SPCE shows peaks comparable to those of P-rGO/PB/SPCE, with increased peak intensity for the C−O−C and C═O bonds due to the SOxENs. The O1s spectra (Fig. S3b) of bare SPCE exhibits two significant peaks at 532.7 and 535.7 eV to indicate the C═O and C−O functionalities, whereas PB/SPCE shows only one peak at 532.1 eV (C═O). P-rGO/SPCE and P-rGO/PB/SPCE show C═O and C−O peaks, respectively. SOxENs/PB/SPCE exhibits peaks similar to those of P-rGO/PB/SPCE, and a new peak at 532.1 eV, representing the O−C═O bond due to SOx [25].

The Fe2p spin-orbit doublet spectra (Fig. 3a) of PB/SPCE and P-rGO/PB/SPCE demonstrate five notable peaks at 708.4, 709.7, 714.2, 721.2, and 724.1 eV, assigned to the $Fe^{II}2p3/2$ (FeCN), $Fe^{III}2p3/2$, Fe satellite, $Fe^{II}2p1/2$, and $Fe^{III}2p1/2$ peaks, respectively. The characteristic Fe^{3+} and Fe^{2+} peaks (mixed-valence states) originate from PB. SOxENs/PB/SPCE exhibits peaks similar to those of P-rGO/PB/SPCE, accompanied by a diminished Fe satellite peak due to the dense SOxENs layer over PB. The N1s spectrum (Fig. 3b) of PB/SPCE is deconvoluted into two peaks at 397.8 and 398.8 eV, which suggest the C≡N bonds of PB and pyrrolic N bonds respectively [26]. P-rGO/PB/SPCE features the same peaks as PB/SPCE, with an additional peak at 400.1 eV (pyridinic N-oxide bonds), owing to the PSSL in P-rGO. SOxENs/PB/SPCE reveals the same three peaks as P-rGO/PB/SPCE, and the predominant pyrrolic N bonds indicate that the nitrogen atoms exist mainly in SOx.

The S2p spectra (Fig. 4) of P-rGO/SPCE, P-rGO/PB/SPCE, and SOxENs/PB/SPCE exhibit a set of doublet peaks with varying

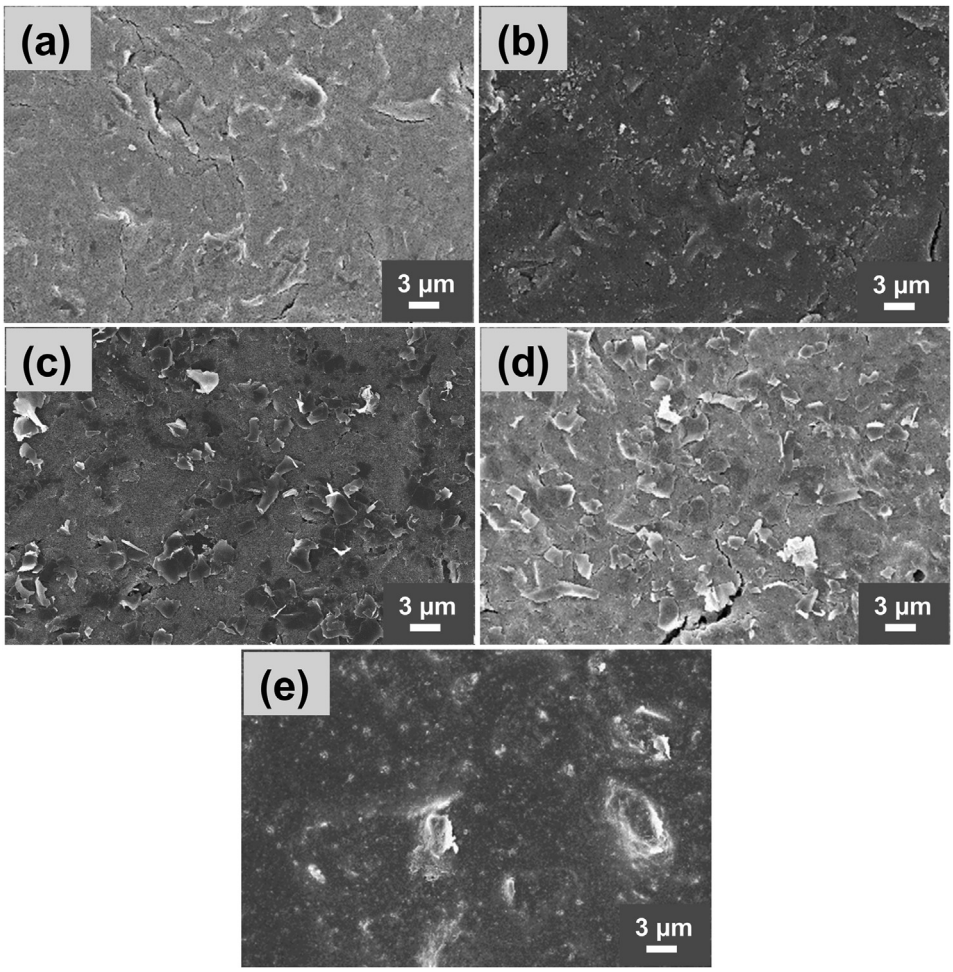

Fig. 1. FE-SEM illustrations of (a) bare SPCE, (b) PB/SPCE, (c) P-rGO/SPCE, (d) P-rGO/PB/SPCE, and (e) SOxENs/PB/SPCE.

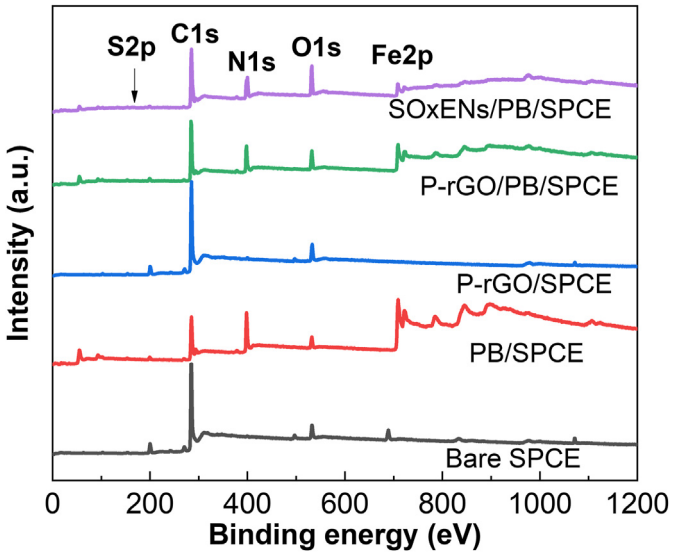

Fig. 2. XPS survey scan of all the modified biosensors.

intensities. The P-rGO/SPCE has two main peaks centered at 163.6 and 164.6 eV, which feature the C–S–C and C=S bonds of the disulfide groups in the PSSL, respectively. Two additional small peaks at 167.9 and 169.2 eV are ascribed to the sulfonate (C–SO_3–C) groups and oxidized S moieties, respectively [27]. P-rGO/PB/SPCE reveals four similar peaks, and the C–SO_3–C peak is predominant over the other peaks. SOxENs/PB/SPCE also shows C=S, C–S–C, C–SO_3–C, and oxidized S moieties. Moreover, the peak intensity of oxidized S moieties increases due to SOx. Therefore, the XPS results confirm the successful formation and chemical interactions between PB, P-rGO, and SOx.

3.2. Electrochemical performance of the differently modified biosensors

The electrochemical performance of various biosensors (bare SPCE, PB/SPCE, P-rGO/SPCE, P-rGO/PB/SPCE, and SOxENs/PB/SPCE) was evaluated by CV experiments. Fig. 5a shows the cyclic voltammograms of the biosensors in 5 mM $K_3[Fe(CN)_6]$ prepared using 100 mM KCl at 50 mV s^{-1}. In addition, the anodic peak currents (i_{pa}) were measured and plotted for the various modified electrodes (Fig. 5b). The i_{pa} values for bare SPCE, PB/SPCE, P-rGO/SPCE, P-rGO/PB/SPCE, and SOxENs/PB/SPCE were 63.6, 158.9, 56.9, 231.7, and 154.5 μA, respectively. Bare SPCE reveals redox peaks, which are very clearly visible or well-defined. In comparison, PB/SPCE, P-rGO/PB/SPCE, and SOxENs/PB/SPCE showed increased i_{pa} values, indicating that PB, P-rGO, and SOxENs all improve the specific surface area of the biosensor. In comparison with P-rGO/PB/SPCE, the SOxENs/PB/SPCE biosensor exhibited a slightly decreased i_{pa} value

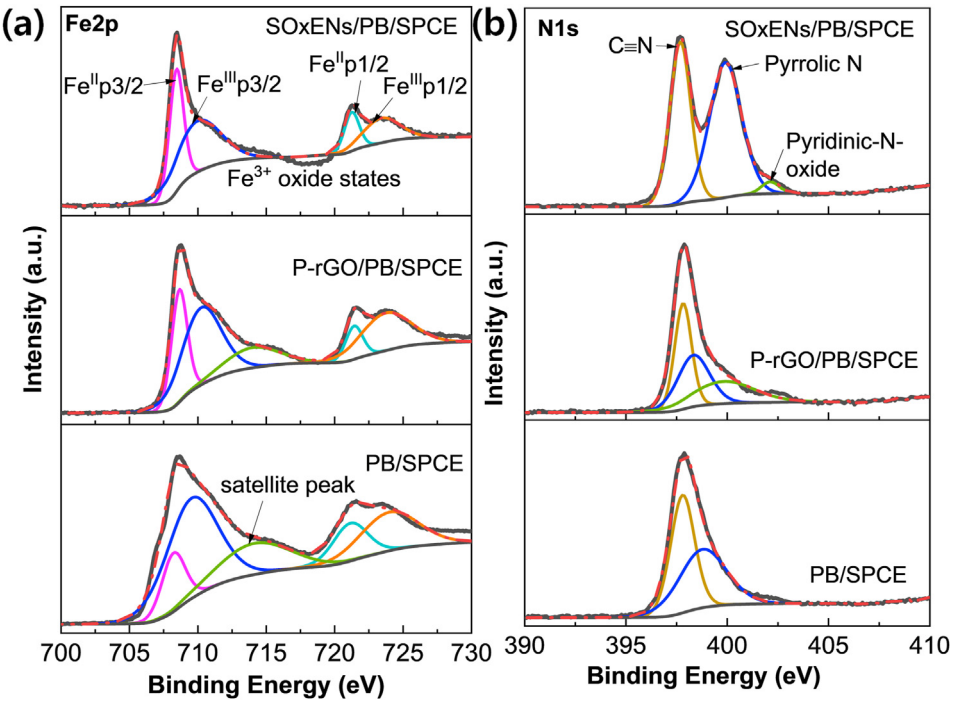

Fig. 3. Deconvoluted high-resolution (a) Fe2p and (b) N1s spectra of all the modified biosensors.

with potential shifts towards negative regions. This is due to a thicker interface and the presence of carboxylate groups in SOxENs, which provide a net negative charge that blocks or repels the negatively charged $K_3[Fe(CN)_6]$ redox probe toward the biosensors [28].

Electron transfer kinetics of the differently modified biosensors was also evaluated at different scan rates (5, 10, 25, 50, 75, and 100 mV s^{-1}) using the CV technique. The anodic (E_{pa}) and cathodic peak potentials (E_{pc}) reveal notable shifts, with the general trend of gradually growing peak currents when the scan rate increases. The i_{pa} and cathodic peak current (i_{pc}) values were measured and plotted against the square root of the scan rates (data not shown). For PB/SPCE, P-rGO/PB/SPCE, and SOxENs/PB/SPCE, the ratio of i_{pa} to i_{pc} was close to 1, and the peak-to-peak separation (ΔE_p) increased proportionally with the scan rate. These characteristics suggest that the redox reaction is a quasi-reversible electron transfer process. The electrochemically active surface area (ECSA) was calculated by the Randles–Ševčík equation [29].

$$i_{pa} = 2.69 \times 10^5 n^{3/2} A C D^{1/2} \nu^{1/2} \quad (3)$$

where i_{pa} is the anodic peak current (A), n: the number of electrons transferred (n = 1), A: the ECSA (cm^2), D: the diffusion coefficient (0.04472 cm^2 s^{-1}), C: the concentration of the redox probe (M), and ν: the scan rate (V s^{-1}). According to this equation, the ECSA values of PB/SPCE (0.257 cm^2) and SOxENs/PB/SPCE (0.219 cm^2) are twice that of the bare SPCE (0.126 cm^2), whereas that of P-rGO/SPCE (0.118 cm^2) was similar to that of bare SPCE. Remarkably, the ECSA of P-rGO/PB/SPCE (0.502 cm^2) was four times that of the bare SPCE, indicating improved conductivity due to the synergistic effects PB and P-rGO.

EIS was used to determine electron transfer properties of the modified electrodes at the solution interface. The different processes taking place at the electrochemical interface (i.e., capacitive, resistive, diffusion effects) across the wide frequency range could be studied. The crucial parameters used in equivalent circuits are the solution resistance (R_s), charge-transfer resistance (R_{CT}), double-layer capacitance C_{CPE}, and Warburg element capacitance (C_W) [30]. Fig. 5c represents the typical Nyquist plots for all the modified electrodes. The collected EIS results was fitted using an appropriate Randles circuit R(C(RW) for the bare SPCE and R(C(RW))(CR) for the PB/SPCE, and P-rGO/SPCE. The P-rGO/PB/SPCE, and SOxENs/PB/SPCE were fitted using R(C(RW))(CR)(CR) and the fitted parameters are given in Table S1. Comparing the bare SPCE and other four modifications, the R_s value was slightly changed by 10% which indicates that the various modifications of the SPCE have no effect at the solution interface. A semi-circular region at higher frequencies corresponds to the process limited by R_{CT}, and a linear lower part at lower frequencies corresponds to the diffusion process as per the C_W. The decreased R_{CT} values of PB/SPCE (0.7 kΩ cm^{-2}) and P-rGO/PB/SPCE (0.4 kΩ cm^{-2}) demonstrate enhanced electron transfer properties, whereas the increased R_{CT} of P-rGO/SPCE (5.9 kΩ cm^{-2}) and bare SPCE (3.1 kΩ cm^{-2}) reveal a much decreased electron transfer rate [31]. The slightly increased R_{CT} value of SOxENs/PB/SPCE (1.9 Ω cm^{-2}) is attributed to the entrapment of SOx. Although the SO_X biomolecule has insulating properties that might impede electron transfer, this R_{CT} value is smaller in comparison with bare SPCE, suggesting that the desired electron transfer is feasible. As the PSSL contains electronegative sulfonate groups, it could improve the electron transfer and diffusion of the redox probe toward the electrode [32]. In comparison with bare SPCE, the C_W for PB/SPCE was decreased by 26% and increased by 42%, 8%, and 14% for the P-rGO/SPCE, P-rGO/PB/SPCE, and SOxENs/PB/SPCE, respectively. In comparison with bare SPCE, the C_{CPE} for PB/SPCE was increased by 74% and for the P-rGO/SPCE, P-rGO/PB/SPCE, and SOxENs/PB/SPCE the increase was by 9%, 174%, and 160%, respectively. The magnitudes of changes of the C_W and C_{CPE} parameters in the electrolyte solution is strongly influenced by the PB, P-rGO, and SOxENs layers. These results emphasize the fact that P-rGO/PB/SPCE, PB/SPCE, and SOxENs/PB/SPCE have remarkable electron transfer properties, which facilitate fast electron transfer kinetics in comparison with bare SPCE. Furthermore, the

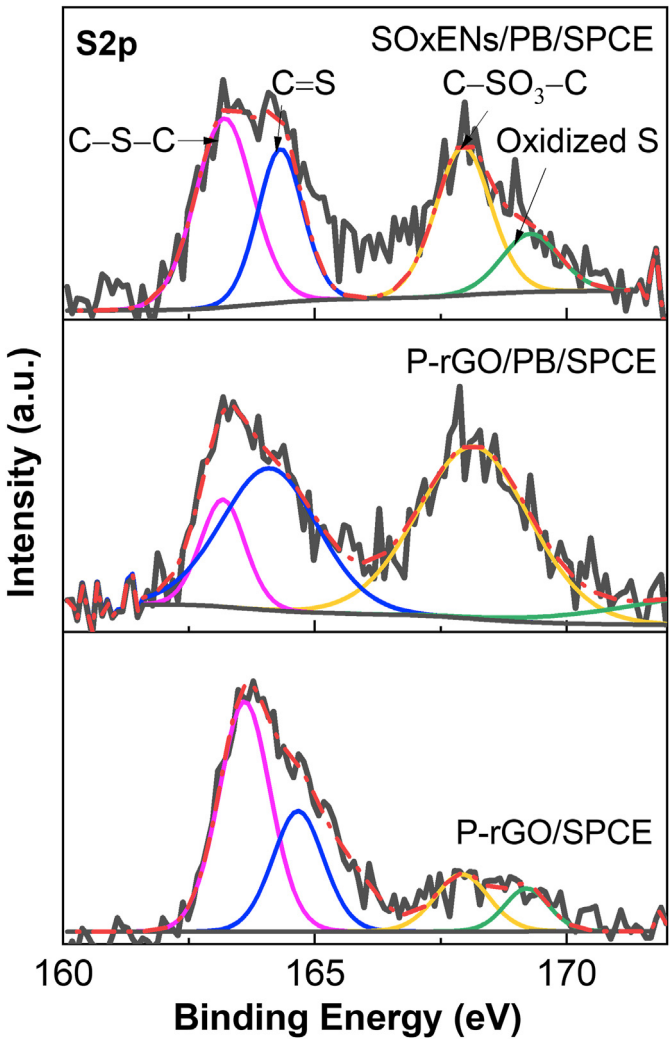

Fig. 4. Deconvoluted high-resolution S2p spectra of all the modified biosensors.

EIS results are in good agreement with the CV results. Therefore, these results also demonstrate improved conductivity of the biosensor by the integration of PB and P-rGO.

3.3. Optimization of biosensor performance

To identify the conditions for optimum biosensor performance, CA experiments were carried out on bare SPCE, PB/SPCE, P-rGO/SPCE, and P-rGO/PB/SPCE for H_2O_2. The amperometric current responses were measured 10 s after each successive H_2O_2 addition at various concentrations (0, 25, 50, 100, 150, and 200 μM), and the calibration plots are shown in Fig. S4. Bare SPCE and P-rGO/SPCE showed no noticeable changes in the current responses, whereas PB/SPCE and P-rGO/PB/SPCE demonstrate significant current responses with increasing H_2O_2 concentration. Moreover, the sensitivity of each biosensor was evaluated using the steady-state current calibration curves. In particular, the sensitivities of P-rGO/PB/SPCE and PB/SPCE were estimated to be 4.6 and 4.0 mA mM^{-1} cm^{-2}, whereas those of bare SPCE and P-rGO/SPCE were 0.003 and 0.02 mA mM^{-1} cm^{-2}, respectively. The sensitivity of P-rGO/PB/SPCE is superior to all other biosensors for H_2O_2 detection because of the synergistic interactions between PB and P-rGO. Therefore, P-rGO/PB/SPCE was used for constructing the Sar biosensor.

The Sar biosensor construction further requires concentration optimization of SOx enzyme, the applied potential, and the solution pH. First, we varied the concentration of SOx (0.1, 0.2, 0.4, 0.6, and 0.8 mg/mL) with P-rGO to prepare the SOxENs. As shown in Fig. S5a, the amperometric current responses increased as the enzyme concentration increased from 0.1 to 0.4 mg/mL, while it decreased at 0.6 and 0.8 mg/mL. Thus, 0.4 mg/mL SOx were chosen due to the maximum enzyme bioactivity.

For applied potential optimization, the amperometric experiments were repeated with 200 μM Sar on modified electrodes with and without enzyme at the applied potential range (0.0 to −0.20 V). From the results (Fig. S5b), P-rGO/PB/SPCE exhibited no observable changes in its cathodic current in response to Sar. For SOxENs/PB/SPCE, the cathodic current response increased when the applied potential became more negative. However, to minimize possible interferences in the more negative regions, −0.1 V was selected as the optimal working potential.

The influence of pH on SOxENs/PB/SPCE was tested using 50 mM PBS at different pH values (6.0, 6.5, 7.0, 7.4, and 8.0). On adding Sar, the maximum current results were attained at pH 8.0, which was selected as the suitable working pH in following experiments (Fig. S5c). Another study reported that SOx show maximum catalytic activity and stability at pH 8.0 [9], which is in good agreement with our results. Moreover, PB modified biosensor has been proved stable without any hydrolysis in this pH value [33]. These optimization experiments confirmed that enhanced electrochemical performance with high stability could be achieved in SOxENs/PB/SPCE under the conditions of 0.4 mg/mL SOx, pH 8.0, and −0.1 V potential.

3.4. Sar calibration plots

CA measurements were performed with various concentrations of Sar (0, 10, 25, 50, 75, 100, 200, 300, and 400 μM) using SOxENs/PB/SPCE under the optimized working conditions to obtain the calibration curve. The current responses increased rapidly with increased Sar concentrations, and hence, each response was measured after only 10 s. As shown in Fig. 6a, the obtained amperometric responses were stable and directly proportional to the added concentration of Sar. The calibration curve is shown in Fig. 6b, with the error bars indicating the standard deviation of four mean values. The regression line was obtained as $i = 0.00114\ C_{Sar}$ (μM) − 0.07742 (R^2: 0.9898). Through the obtained calibration, the linear dynamic range was estimated as 10−400 μM, and the sensitivity was calculated to be 9.04 μA mM^{-1} cm^{-2}. The limit of detection (LOD) was 0.66 μM (S/N = 3), which is better than the previously reported amperometric detection of Sar [9] and comparable with other studies [7,8]. The PSSL in P-rGO prevents easy denaturation of SOx, thereby increasing its bioactivity. However, the other studies used highly negative potentials of −0.7 and −0.55 V, while the potential of −0.1 V used here is very low and sufficient for minimizing possible interfering signals from human urine samples [9,34]. Moreover, the applied potential of 1.0 V utilized in a previous study [4] focused on measuring the oxidation current, whereas in this study, the reduction current at −0.1 V (the near zero range) was measured.

Additionally, amperometric current responses were measured after 10 s of successive additions of Sar at various concentrations (0, 10, 25, 50, 100, 200, 300, 400, and 500 μM) for variously modified biosensors, and the calibration plots are shown in Fig. 6c. Note that SOxENs/PB/SPCE demonstrated maximum current responses upon Sar additions, whereas the other biosensors showed no significant increase in their current responses. The relevant parameters of various amperometric Sar biosensors are listed in Table 1.

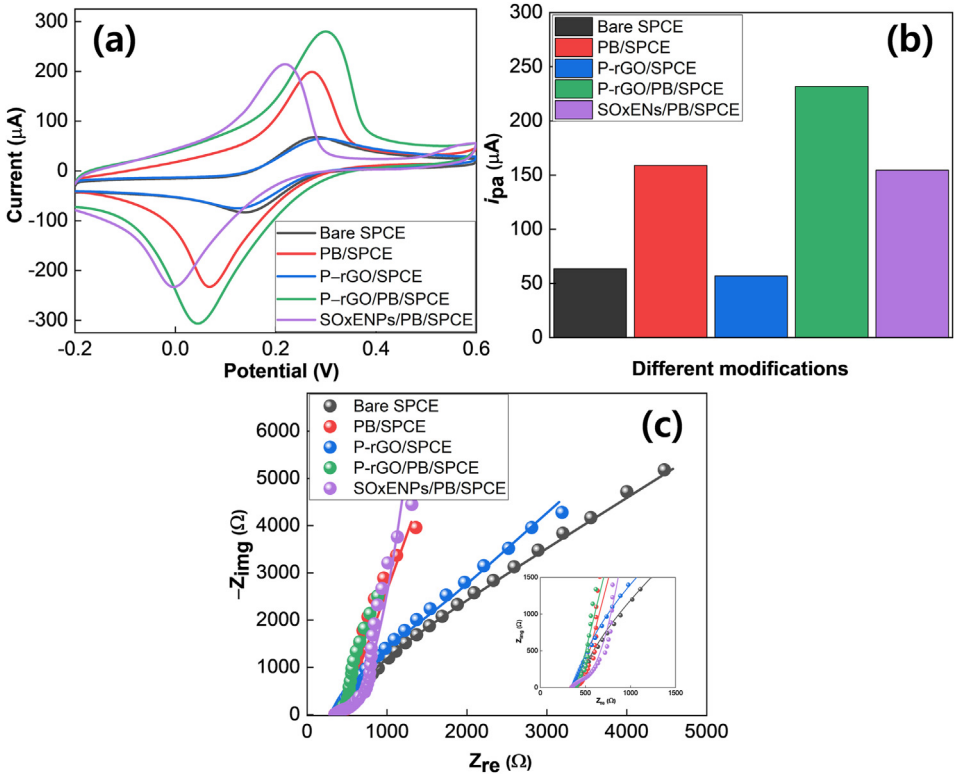

Fig. 5. (a) CV results of the different biosensors (bare SPCE, PB/SPCE, P-rGO/SPCE, P-rGO/PB/SPCE, and SOxENs/PB/SPCE) in 5 mM $K_3[Fe(CN)_6]$ solution containing 100 mM KCl at the scan rate of 50 mV s^{-1}, (b) from the CV results, i_{pa} values measured for all the modified biosensors, and (c) EIS responses of the biosensors in the same solution.

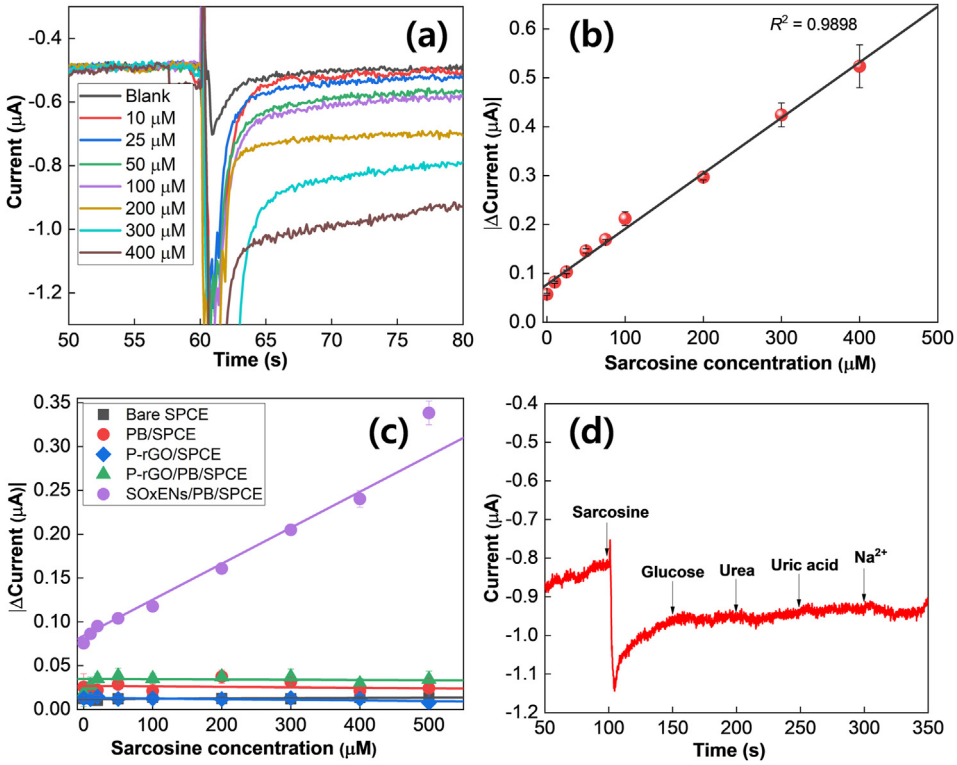

Fig. 6. (a) Amperometric responses of SOxENs/PB/SPCEs in 0.05 M PBS (pH 8.0) with successive additions of different concentrations of Sar at −0.1 V. (b) The Sar calibration curves attained against (a). (c) Calibration plots obtained for the differently modified electrodes through CA experiments in 50 mM PBS (pH 8.0) with successive additions of different concentrations of Sar (0, 25, 50, 75, 100, 200, 300, 400, and 500 μM). (d) Chronoamperometry experiment results of SOxENs/PB/SPCE in PBS (pH 8.0) at −0.1 V, with inclusion of 0.2 mM Sar, glucose, urea, uric acid, and sodium ions.

Table 1
Comparison of parameters for various amperometric Sar biosensors.

Electrode	Applied potential	Linear range (μM)	LOD (μM)	Sensitivity (μA mM^{-1} $cm^{-2)}$	Reference
SOx/Pt/OIHMMP/GCE	0.3 V *vs.* SCE	1.0–70	0.13	231.5	[35]
SOxENPs/AuE	1.0 *vs.* Ag/AgCl	0.1–100	0.01	–	[4]
SOx/Pt/MNP/GCE	0.4 V *vs.* SCE	5.0–40	0.24	123.51	[7]
SOx/SPCE	0.6 *vs.* Ag/AgCl	0.01–0.1	0.016	–	[6]
SOx/Pt@ZIF8/Nafion	0.4 V *vs.* SCE	5.0–30	1.06	57.04	[10]
SOx/PVA–Au–pphTEOS	0.55 *vs.* Ag/AgCl	500–7500	500	40.13	[9]
SOx/polyaniline film	0.4 V *vs.* SCE	100–1000	–	–	[36]
SOx/polypyrrole film	0.4 V *vs.* SCE	100–1000	–	–	[37]
SOx/PAA/GCE	−0.55 *vs.* Ag/AgCl	0.001–0.05	0.0004	–	[38]
Pt–Fe_3O_4@C/GCE	0.3 V *vs.* SCE	0.5–60	0.43	48.8	[8]
SOx/MXene–Chi/GCE	−0.7 *vs.* Ag/AgCl	0.036–7.8	0.018	–	[34]
SOxENs/PB/SPCE	−0.1 *vs.* Ag/AgCl	10–400	0.66	9.04	This work

Pt: platinum, OIHMMP: organic–inorganic hybrid mesoporous molybdenum phosphonate, GCE: glassy carbon electrode, SOxENPs: SOx enzyme nanoparticles AuE: gold electrode, MNP: mesoporous nickel phosphonate, ZIF8: zeolitic imidazolate framework-8, PVA–Au–pphTEOS: polyvinyl alcohol–gold nanoparticles–partially prehydrolyzed tetraethyl orthosilicate, PAA: polyamic acid, Fe_3O_4@C: iron(II,III) oxide@carbon, MXene: transition metal carbides, Chi: chitosan.

3.5. Interference study

Anti-interference or selectivity is an important characteristic for the clinical application of biosensors. The Sar sensing ability of SOxENs/PB/SPCE was studied in the presence of interfering species. As shown in Fig. 6d, the biosensor displayed a rapid current response to Sar, whereas the co-existing electroactive species such as glucose, urea, uric acid, and Na^{2+} ions had no impact because of the substrate specificity of SOx. In particular, the anti-interference ability of the biosensor is attributed to the electronegative sulfonate groups in the PSSL, which repel negatively charged species such as uric acid and reduce the interfering signals [24]. These results demonstrate the superior selectivity of SOxENs/PB/SPCE toward Sar.

3.6. Stability and reproducibility studies

The shelf life of the biosensors was investigated through CA experiments using 200 μM Sar. The biosensors were stored dry at 4 °C for up to 21 days. The biosensors (n = 5) were tested weekly once and exhibited approximately 17% loss in the initial current response after one week and 43% loss after 3 weeks (Fig. S6a). The storage stability is assumed to be due to the use of P-rGO frame for enzyme immobilization. Five identically prepared SOxENs/PB/SPCE biosensors were also utilized to evaluate the reproducibility between the electrodes and within the electrodes. The relative standard deviation estimated as 5% was from three replicate measurements of the five electrodes as shown in Fig. S6b. Therefore, the biosensors exhibited good stability and reproducibility for Sar detection.

3.7. Real sample analysis

The clinical applicability of the fabricated biosensor was evaluated by determining Sar concentration in urine samples from both healthy humans and PCa patients using the method of standard addition. The CA method for the typical calibration curve plots was followed except that the urine samples were used instead of Sar solution. The measured Sar concentration in the urine of healthy humans was 10.6 μM, whereas that in the PCa samples was 35.1 μM (n = 4). Recoveries from PCa urine samples spiked with 10, 25, and 50 μM Sar were 101.7%, 106.8%, and 102.2%, respectively, and the results are summarized in Table 2. The Sar concentration in PCa urine samples was approximately 3.3 times higher than that of the normal samples, suggesting an increased Sar concentration in the urine of PCa patients. To evaluate the reliability of the biosensor, the results were compared with measurements using the standard calorimetric assay kit. From the standard curve obtained following the kit protocol, the Sar concentrations of the apparently normal and PCa patients were 10.6 and 32.3 μM, respectively. There was a good correlation between the biosensor and assay kit results, indicating the feasibility of the biosensor for Sar detection in clinical applications.

4. Conclusions

The proposed SOxENs/PB/SPCE biosensor is simple and effective for Sar determination in clinical samples amidst various co-existing species. PB functions as a signal transducer boosting the sensitivity of the fabricated biosensor in H_2O_2 concentration evaluation. The P-rGO with enhanced electrocatalytic activity and surface area ensured highly efficient enzyme loading and rapid mass transport. We observed that the SOxENs layer is more stable over the electrode due to the excellent adhesive properties of PSSL. The biosensor features a sensitivity of 9.04 μA mM^{-1} cm^{-2}, a wide linear range (10–400 μM), and a low LOD (0.66 μM) for Sar detection at a very low applied potential of −0.1 V. The low working potential applied not only improves the selectivity towards Sar but also reduces the electrochemical activity of major interfering compounds. The developed biosensor thus possesses satisfactory

Table 2
Comparison of Sar concentrations measured in human urine samples.

Methods	Added (μM)	Found (μM)	+SD (μM)	Recovery (%)	RSD (%)
Proposed biosensor	Normal	10.9	0.001		11.9
	PCa	35.1	0.006		15.9
	10	45.9	0.008	101.7	15.1
	25	75.8	0.012	106.8	14.4
	50	128.6	0.018	102.2	12.5
Colorimetric assay kit	Normal	10.6			
	PCa	32.3			

SD: standard deviation, RSD: relative standard deviation.

anti-inference features, good precision or stability over 3 weeks, and high reproducibility. The biosensor when applied to urine samples from both healthy humans and PCa patients, the results were in good agreement with the standard colorimetric assay kit results, proving the accuracy of the biosensor. Therefore, the designed biosensor is a promising candidate for non-invasive PCa diagnosis.

CRediT authorship contribution statement

Thenmozhi Rajarathinam: Writing – original draft, Conceptualization, Methodology, Data curation, Investigation, Validation. **Minho Kwon:** Conceptualization, Methodology, Data curation, Investigation, Validation. **Dinakaran Thirumalai:** Conceptualization, Methodology, Writing – review & editing, Supervision, Validation, Software. **Seonghye Kim:** Methodology, Investigation, Validation. **Seulah Lee:** Methodology, Investigation, Validation. **Jang-Hee Yoon:** Methodology, Investigation. **Hyun-jong Paik:** Conceptualization, Methodology, Supervision, Validation. **Suhkmann Kim:** Supervision, Validation, Funding acquisition. **Jaewon Lee:** Methodology, Supervision, Validation. **Hong Koo Ha:** Project administration, Supervision, Validation, Funding acquisition. **Seung-Cheol Chang:** Conceptualization, Methodology, Project administration, Supervision, Investigation, Validation.

Declaration of competing interest

The authors declare the following financial interests/personal relationships which may be considered as potential competing interests: Seung-Cheol Chang reports financial support was provided by National Research Foundation of Korea. Suhkmann Kim reports financial support was provided by Korea Ministry of Oceans and Fisheries. Hyun-jong Paik reports financial support was provided by National Research Foundation of Korea.

Acknowledgements

This work was supported by a National Research Foundation of Korea (NRF) grant funded by the Korean government (MSIT) (No. NRF-2019R1F1A1063034). This study was part of the project titled “Omics based on fishery disease control, technology development, and industrialization (20150242)” funded by the Ministry of Oceans and Fisheries, Korea. This research was also supported by Nano-Material Technology Development Program through the National Research Foundation of Korea (NRF) funded by the Ministry of Science, ICT and Future Planning (2017M3A7B4014045).

Appendix A. Supplementary data

Supplementary data to this article can be found online at https://doi.org/10.1016/j.aca.2021.338749.

References

[1] J.R. Prensner, M.A. Rubin, J.T. Wei, A.M. Chinnaiyan, Beyond PSA: the next generation of prostate cancer biomarkers, Sci. Transl. Med. 4 (2012) 127rv3, https://doi.org/10.1126/scitranslmed.3003180.
[2] C.E. Baum, D.K. Price, W.D. Figg, Sarcosine as a potential prostate cancer biomarker and therapeutic target, Canc. Biol. Ther. 9 (2010) 341–342, https://doi.org/10.4161/cbt.9.5.11310.
[3] N. Cernei, O. Zitka, M. Ryvolova, V. Adam, M. Masarik, J. Hubalek, R. Kizek, Spectrometric and electrochemical analysis of sarcosine as a potential prostate carcinoma marker, Int. J. Electrochem. Sci. 7 (2012) 4286–4301.
[4] P. Kumar, V. Narwal, R. Jaiwal, C.S. Pundir, Construction and application of amperometric sarcosine biosensor based on SOxNPs/AuE for determination of prostate cancer, Biosens. Bioelectron. 122 (2018) 140–146, https://doi.org/10.1016/j.bios.2018.09.003.
[5] A. Ramanavicius, Amperometric biosensor for the determination of creatine, Anal. Bioanal. Chem. 387 (2007) 1899–1906, https://doi.org/10.1007/s00216-006-1065-2.
[6] T.S.C.R. Rebelo, C.M. Pereira, M.G.F. Sales, J.P. Noronha, J. Costa-Rodrigues, F. Silva, M.H. Fernandes, Sarcosine oxidase composite screen-printed electrode for sarcosine determination in biological samples, Anal. Chim. Acta 850 (2014) 26–32, https://doi.org/10.1016/j.aca.2014.08.005.
[7] Q. Wang, C. Yang, Q. Yang, S. Yu, H. Yang, Platinum-loaded mesoporous nickel phosphonate and its electrochemical application for sarcosine detection, Anal. Chim. Acta 1046 (2019) 93–98, https://doi.org/10.1016/j.aca.2018.09.027.
[8] Q. Yang, N. Li, Q. Li, S. Chen, H.L. Wang, H. Yang, Amperometric sarcosine biosensor based on hollow magnetic Pt-Fe3O4@C nanospheres, Anal. Chim. Acta 1078 (2019) 161–167, https://doi.org/10.1016/j.aca.2019.06.031.
[9] U. Lad, G.M. Kale, R. Bryaskova, Sarcosine oxidase encapsulated polyvinyl alcohol-silica-AuNP hybrid films for sarcosine sensing electrochemical bioelectrode, J. Electrochem. Soc. 161 (2014) B98–B101, https://doi.org/10.1149/2.018405jes.
[10] H. Yang, J. Wang, C. Yang, X. Zhao, S. Xie, Z. Ge, Nano Pt@ZIF8 modified electrode and its application to detect sarcosine, J. Electrochem. Soc. 165 (2018) H247–H250, https://doi.org/10.1149/2.1231805jes.
[11] A.A. Karyakin, Advances of Prussian blue and its analogues in (bio) sensors, Curr. Opin. Electrochem. 5 (2017) 92–98, https://doi.org/10.1016/j.coelec.2017.07.006.
[12] D. Thirumalai, S. Kim, S. Kim, S.C. Chang, Reagentless amperometric pyruvate biosensor based on a Prussian blue- and enzyme nanoparticle-modified screen-printed carbon electrode, ACS Omega 5 (2020) 30123–30129, https://doi.org/10.1021/acsomega.0c04522.
[13] J. Pena-Bahamonde, H.N. Nguyen, S.K. Fanourakis, D.F. Rodrigues, Recent advances in graphene-based biosensor technology with applications in life sciences, J. Nanobiotechnol. 16 (2018) 75, https://doi.org/10.1186/s12951-018-0400-z.
[14] M. Thangamuthu, K.Y. Hsieh, P.V. Kumar, G.Y. Chen, Graphene- and graphene oxide-based nanocomposite platforms for electrochemical biosensing applications, Int. J. Mol. Sci. 20 (2019) 2975, https://doi.org/10.3390/ijms20122975.
[15] A. Liang, X. Jiang, X. Hong, Y. Jiang, Z. Shao, D. Zhu, Recent developments concerning the dispersion methods and mechanisms of graphene, Coatings 8 (2018) 33, https://doi.org/10.3390/coatings8010033.
[16] S. Stankovich, R.D. Piner, X. Chen, N. Wu, S.T. Nguyen, R.S. Ruoff, Stable aqueous dispersions of graphitic nanoplatelets via the reduction of exfoliated graphite oxide in the presence of poly(sodium 4-styrenesulfonate), J. Mater. Chem. 16 (2006) 155–158, https://doi.org/10.1039/b512799h.
[17] H. Bai, Y. Xu, L. Zhao, C. Li, G. Shi, Non-covalent functionalization of graphene sheets by sulfonated polyaniline, Chem. Commun. (2009) 1667–1669, https://doi.org/10.1039/b821805f.
[18] W. Zhu, J. Ma, X. Nan, P.O. Lartey, Y. Yang, Study on dispersion of reduced graphene oxide on physical performance of polyvinylidene fluoride composites by hansen solubility parameters, Colloid Polym. Sci. 297 (2019) 213–224, https://doi.org/10.1007/s00396-018-4456-y.
[19] E.Y. Choi, T.H. Han, J.H. Hong, J.E. Kim, S.H. Lee, H.W. Kim, et al., Noncovalent functionalization of graphene with end-functional polymers, J. Mater. Chem. 20 (2010) 1907–1912, https://doi.org/10.1039/b919074k.
[20] X. Qi, K.Y. Pu, H. Li, X. Zhou, S. Wu, Q.L. Fan, et al., Amphiphilic graphene composites, Angew. Chem., Int. Ed. Engl. 49 (2010) 9426–9429, https://doi.org/10.1002/anie.201004497.
[21] H. Wang, S.G. Bi, Y.S. Ye, Y. Xue, X.L. Xie, Y.W. Mai, An effective non-covalent grafting approach to functionalize individually dispersed reduced graphene oxide sheets with high grafting density, solubility and electrical conductivity, Nanoscale 7 (2015) 3548–3557, https://doi.org/10.1039/c4nr06710j.
[22] S. Lee, J.-S. Yeo, J.-M. Yun, D.-Y. Kim, Water dispersion of reduced graphene oxide stabilized via fullerenol semiconductor for organic solar cells, Opt. Mater. Express 7 (2017) 2487–2495, https://doi.org/10.1364/ome.7.002487.
[23] K. Zargoosh, M.J. Chaichi, M. Shamsipur, S. Hossienkhani, S. Asghari, M. Qandalee, Highly sensitive glucose biosensor based on the effective immobilization of glucose oxidase/carbon-nanotube and gold nanoparticle in Nafion film and peroxyoxalate chemiluminescence reaction of a new fluorophore, Talanta 93 (2012) 37–43, https://doi.org/10.1016/j.talanta.2011.11.029.
[24] D. Thirumalai, D. Subramani, B. Shin, H.j. Paik, S.C. Chang, A metal-free, non-enzymatic electrochemical glucose sensor with a de-bundled single-walled carbon nanotube-modified electrode, Bull. Kor. Chem. Soc. 39 (2018) 141–145, https://doi.org/10.1002/bkcs.11358.
[25] P. Roy, P.-C. Chen, A.P. Periasamy, Y.-N. Chen, H.-T. Chang, Photoluminescent carbon nanodots: synthesis, physicochemical properties and analytical applications, Mater. Today Off. 18 (2015) 447–458, https://doi.org/10.1016/j.mattod.2015.04.005.
[26] M. Eryiğit, E. Temur, T.Ö. Özer, H.Ö. Doğan, Electrochemical fabrication of Prussian blue nanocube-decorated electroreduced graphene oxide for amperometric sensing of NADH, Electroanalysis 31 (2019) 905–912, https://doi.org/10.1002/elan.201800830.
[27] C. Bautista-Flores, J.S. Arellano-Peraza, R.Y. Sato-Berrú, E. Camps, D. Mendoza, Sulfur and few-layer graphene interaction under thermal treatments, Chem. Phys. Lett. 665 (2016) 121–126, https://doi.org/10.1016/j.cplett.2016.10.056.
[28] F. Tasca, W. Harreither, R. Ludwig, J.J. Gooding, L. Gorton, Cellobiose dehydrogenase aryl diazonium modified single walled carbon nanotubes: enhanced direct electron transfer through a positively charged surface, Anal. Chem. 83 (2011) 3042–3049, https://doi.org/10.1021/ac103250b.

[29] D. Thirumalai, V. Kathiresan, J. Lee, S.H. Jin, S.C. Chang, Electrochemical reactive oxygen species detection by cytochrome c immobilized with vertically aligned and electrochemically reduced graphene oxide on a glassy carbon electrode, Analyst 142 (2017) 4544, https://doi.org/10.1039/c7an01387f, 4452.
[30] A. Ramanavicius, P. Genys, A. Ramanaviciene, Electrochemical impedance spectroscopy based evaluation of 1,10-Phenanthroline-5,6-dione and glucose oxidase modified graphite electrode, Electrochim. Acta 146 (2014) 659–665, https://doi.org/10.1016/j.electacta.2014.08.130.
[31] A. Valiūnienė, A.I. Rekertaitė, A. Ramanavičienė, L. Mikoliūnaitė, A. Ramanavičius, Fast Fourier transformation electrochemical impedance spectroscopy for the investigation of inactivation of glucose biosensor based on graphite electrode modified by Prussian blue, polypyrrole and glucose oxidase, Colloids Surf. A Physicochem. Eng. Asp. 532 (2017) 165–171, https://doi.org/10.1016/j.colsurfa.2017.05.048.
[32] C. Fernández-Sánchez, C.J. McNeil, K. Rawson, Electrochemical impedance spectroscopy studies of polymer degradation: application to biosensor development, TrAC Trends Anal. Chem. (Reference Ed.) 24 (2005) 37–48, https://doi.org/10.1016/j.trac.2004.08.010.
[33] A. Valiūnienė, P. Virbickas, G. Medvikytė, A. Ramanavičius, Urea biosensor based on electrochromic properties of Prussian blue, Electroanalysis 32 (2020) 503–509, https://doi.org/10.1002/elan.201900556.
[34] S. Hroncekova, T. Bertok, M. Hires, E. Jane, L. Lorencova, A. Vikartovska, et al., Ultrasensitive Ti3C2TX MXene/chitosan nanocomposite-based amperometric biosensor for detection of potential prostate cancer marker in urine samples, Processes 8 (2020) 580, https://doi.org/10.3390/pr8050580.
[35] Q. Wang, Y. Zhao, Q. Yang, D. Du, H. Yang, Y. Lin, Amperometric sarcosine biosensor with strong anti-interference capabilities based on mesoporous organic-inorganic hybrid materials, Biosens. Bioelectron. 141 (2019) 111431, https://doi.org/10.1016/j.bios.2019.111431.
[36] Y. Yang, S. Mu, The bioelectrochemical response of the polyaniline sarcosine oxidase electrode, J. Electroanal. Chem. 415 (1996) 71–77, https://doi.org/10.1016/s0022-0728(96)04702-x.
[37] Y. Shi, Y. Yang, J. Kan, S. Mu, Y. Li, Bioelectrochemical properties of sarcosine oxidase immobilized in a polypyrrole film, Biosens. Bioelectron. 12 (1997) 655–659, https://doi.org/10.1016/s0956-5663(97)00020-1.
[38] J. Li, J. Ma, Y. Zhang, Z. Zhang, G. He, An amperometric biosensor for the assay of sarcosine based on the cross coupled chemical and electrochemical reactions with practical applications, J. Electroanal. Chem. 833 (2019) 568–572, https://doi.org/10.1016/j.jelechem.2018.12.036.